Annals of Clinical Microbiology and Antimicrobials

RESEARCH

Open Access

# VIM-encoding $Inc_{pSTY}$ plasmids and chromosome-borne integrative and mobilizable elements (IMEs) and integrative and conjugative elements (ICEs) in *Pseudomonas*

Fangzhou Chen[1,2,3†], Peng Wang[1†], Zhe Yin[1], Huiying Yang[1], Lingfei Hu[1], Ting Yu[1], Ying Jing[1], Jiayao Guan[1], Jiahong Wu[2*] and Dongsheng Zhou[1,3*]

## Abstract

**Background:** The carbapenem-resistance genes $bla_{VIM}$ are widely disseminated in *Pseudomonas*, and frequently harbored within class 1 integrons that reside within various mobile genetic elements (MGEs). However, there are few reports on detailed genetic dissection of $bla_{VIM}$-carrying MGEs in *Pseudomonas*.

**Methods:** This study presented the complete sequences of five $bla_{VIM-2/-4}$-carrying MGEs, including two plasmids, two chromosomal integrative and mobilizable elements (IMEs), and one chromosomal integrative and conjugative element (ICE) from five different *Pseudomonas* isolates.

**Results:** The two plasmids were assigned to a novel incompatibility (Inc) group $Inc_{pSTY}$, which included only seven available plasmids with determined complete sequences and could be further divided into three subgroups $Inc_{pSTY}$-1/2/3. A detailed sequence comparison was then applied to a collection of 15 MGEs belonging to four different groups: three representative $Inc_{pSTY}$ plasmids, two Tn*6916*-related IMEs, two Tn*6918*-related IMEs, and eight Tn*6417*-related ICEs and ten of these 15 MGEs were first time identified. At least 22 genes involving resistance to seven different categories of antibiotics and heavy metals were identified within these 15 MGEs, and most of these resistance genes were located within the accessory modules integrated as exogenous DNA regions into these MGEs. Especially, eleven of these 15 MGEs carried the $bla_{VIM}$ genes, which were located within 11 different concise class 1 integrons.

**Conclusion:** These $bla_{VIM}$-carrying integrons were further integrated into the above plasmids, IMEs/ICEs with intercellular mobility. These MGEs could transfer between *Pseudomonas* isolates, which resulted in the accumulation and spread of $bla_{VIM}$ among *Pseudomonas* and thus was helpful for the bacteria to survival from the stress of antibiotics.

*Correspondence: jiahongw@gmc.edu.cn; dongshengzhou1977@gmail.com; zhouds@bmi.ac.cn
†Fangzhou Chen and Peng Wang contributed equally to this work
[1] State Key Laboratory of Pathogen and Biosecurity, Beijing Institute of Microbiology and Epidemiology, Beijing 100071, China
[2] Basic Medical College, Guizhou Medical University, Guiyang 550025, China
Full list of author information is available at the end of the article

Data presented here provided a deeper insight into the genetic diversification and evolution of VIM-encoding MGEs in *Pseudomonas*.

**Keywords:** *Pseudomonas*, $Bla_{VIM}$, Mobile genetic elements, Integrons, Antibiotic resistance, ST129

## Introduction

VIM hydrolyzes nearly all β-lactam except for aztreonam and currently consists of 76 variants (https://www.ncbi.nlm.nih.gov/pathogens/refgene) [1]. The $bla_{VIM}$ genes are mostly found in *Pseudomonas* and Enterobacteriaceae and occur frequently within class 1 integrons with distinct gene cassette arrays (GCAs). The $bla_{VIM}$-carrying integrons are always presented in various mobile genetic elements (MGEs) such as plasmids, integrative and conjugative elements (ICEs), and integrative and mobilizable elements (IMEs), enhancing the mobility and dissemination of $bla_{VIM}$ genes [2].There are a wealth of sequenced $bla_{VIM}$-carrying plasmids, which can be assigned to various incompatibility (Inc) groups such as IncA, IncC, IncN, IncP and IncL/M [3–7]. IMEs/ICEs are frequently located in bacterial chromosomes: ICEs encode self-conjugation modules and thus are able to transfer between cells [8], whereas IMEs needs a helper conjugative element to achieve intercellular mobility [9].

Our previous studies showed the detailed genetic characteristics of two novel carbapenemase-encoding MGEs: SIM-encoding plasmid pHN39-SIM [10] and $bla_{VIM-4}$-containing ICE Tn*6413* [7]. This follow-up study presented the complete sequences of five novel $bla_{VIM-2/-4}$-carrying MGEs, including two plasmids pJ20133-VIM and p716811-VIM, and two chromosomal IMEs Tn*6917* and Tn*6918*, and one chromosomal ICE Tn*6953* from *Pseudomonas* isolates. These two plasmids were assigned to a novel Inc group $Inc_{pSTY}$. Comprehensive sequence comparisons were then applied to three representative $Inc_{pSTY}$ plasmids and 12 chromosome-borne IMEs and ICEs (including the above five ones), providing a deeper understanding of the genetic diversification and evolution of VIM-encoding MGEs in *Pseudomonas*.

## Materials and methods

### Bacterial strains and identification

Five clinical isolates *P. aeruginosa* SE5443, *P. putida* 716811 and 159349, and *P. monteilii* J20133 and 918607 were collected from four different Chinese public hospitals (Additional file 1: Table S1). The 16S rRNA genes and the $bla_{VIM}$ genes were detected as described previously [7].

### Genomic DNA extraction, sequencing, and sequence assembly

Bacterial genomic DNA was isolated using the Ultra-Clean Microbial Kit (Qiagen, NW, Germany), and sequenced from a sheared DNA library with average size of 15 kb (ranged from 10 to 20 kb) on a PacBio RSII sequencer (Pacific Biosciences, CA, USA), as well as a paired-end library with an average insert size of 350 bp (ranged from 150 to 600 kb) on a HiSeq sequencer (Illumina, CA, USA) [11]. The paired-end short Illumina reads were used to correct the long PacBio reads utilizing proovread [12], and then the corrected PacBio reads were assembled de novo utilizing SMARdenovo (https://github.com/ruanjue/smartdenovo).

### Sequence annotation and comparison

Genome sequences were annotated by the Rapid Annotation using Subsystem Technology (RAST) [13] combined with BLASTP/BLASTX/BLASTN [14], Domain (https://www.ncbi.nlm.nih.gov/Structure/cdd/wrpsb.cgi), and RefSeq database [15]. Annotation of resistance genes, MGEs, and other features were carried out using the online databases including CARD [16], ResFinder [17], ISfinder [18], INTEGRALL [19], and Tn Number Registry [20]. Multiple and pairwise sequence comparisons were performed using BLASTN. Gene organization diagrams were drawn using Inkscape 1.0 (https://inkscape.org/en/).

### Phylogenetic analysis

Indicated nucleotide sequences were aligned using Clustal Omega 1.2.2 [21], and then maximum-likelihood phylogenetic trees were constructed from aligned sequences using MEGA X 10.1.8 [22] with a bootstrap iteration of 1000.

### Conjugal transfer

Each indicated $bla_{VIM}$-carrying MGE was transformed from its wild-type isolate into rifampin-resistant *P. aeruginosa* ATCC 27853 or PAO1, through conjugal transfer or electroporation experiments. Three milliliters of overnight cultures of each donor and recipient bacteria were mixed together, harvested, and resuspended in 80 mL of Brain Heart Infusion (BHI) broth (BD Biosciences). The mixture was spotted on a 1 $cm^2$ hydrophilic nylon

membrane filter with a 0.45 μm pore size (Millipore) that was placed on BHI agar (BD Biosciences) plate and then incubated for mating at 26 °C or 37 °C for 12 h to 18 h. Bacteria were washed from filter membrane and spotted on BHI plates, for selecting a $bla_{VIM}$-carrying transconjugant. 1500 mg/mL rifampin (for ATCC 27853 or PAO1), together with 4 mg/mL meropenem (for $bla_{VIM}$) was used as transconjugant selection.

### Phenotypic assays and multi-locus sequence typing (MLST)

Bacterial antimicrobial susceptibility was tested by Bio-Mérieux VITEK 2, and interpreted as per the 2020 Clinical and Laboratory Standards Institute (CLSI) guidelines [23]. Activity of Amber class A/B/D carbapenemases was determined with a modified CarbaNP test [24]. The sequence types (STs) of *Pseudomonas* isolates were identified according to the online *Pseudomonas* MLST schemes (https://pubmlst.org/organisms).

## Results

### Identification of three STs for *Pseudomonas* isolates

Three different STs, namely ST129, ST17, and ST639, were identified from the five *Pseudomonas* isolates (Additional file 1: Table S1), whose complete genome sequences were determined in this work. *P. putida* 716811 and 159349 belonged to ST129 and ST17, respectively. *P. aeruginosa* SE5443 belonged to ST639. ST129 was a novel ST of *P. putida*. The two *P. monteilii* isolates J20133 and 918607 could not be assigned with any ST types due to lack of *P. monteilii* MLST scheme.

### Proposal of a novel group of $Inc_{pSTY}$ plasmids

Two $bla_{VIM}$-carrying plasmids pJ20133-VIM and p716811-VIM were identified from the complete genome sequences of the two *Pseudomonas* isolates J20133 and 716811 (Additional file 1: Table S1). A novel $Inc_{pSTY}$ group was proposed from a total of seven available fully sequenced single-replicon plasmids (Additional file 1: Table S2; last accessed August 10th 2020) that included the above two plasmids together with five additional ones from GenBank, because these seven plasmids harbored not only homologous *repA* (replication initiation protein) genes together with its iterons (Fig. 1) but also similar backbone gene organizations (Fig. 2). Since the Inc group of plasmids could be divided according to the homology of *repA* genes [25–27], a phylogenetic tree (Fig. 1) was constructed based on the *repA* sequences of these seven plasmids, showing that these seven plasmids

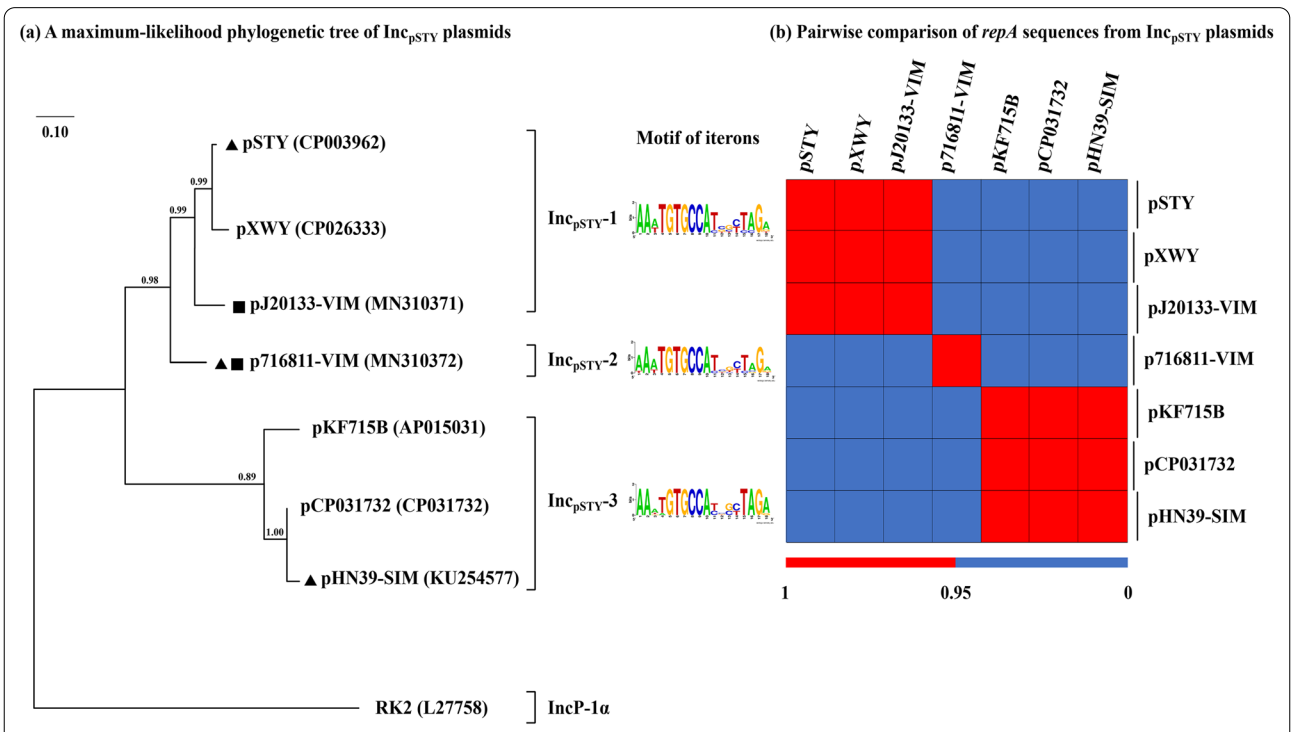


**Fig. 1** Evolutionary relationships of the seven $Inc_{pSTY}$ plasmids. **a** A maximum likelihood phylogenetic tree is constructed from aligned *repA* sequences. IncP-1α plasmid RK2 [60] is used as the outgroup. Degree of support (percentage) for each cluster of associated taxa, as determined by bootstrap analysis, is shown next to each branch. Bar corresponds to scale of sequence divergence. Triangle indicates the reference plasmid of each $Inc_{pSTY}$ subgroup, whilst squares denote the plasmids fully sequenced in this study. **b** A heatmap of pairwise comparison of *repA* sequences. See Table S3 for original BLAST coverage and nucleotide identity values

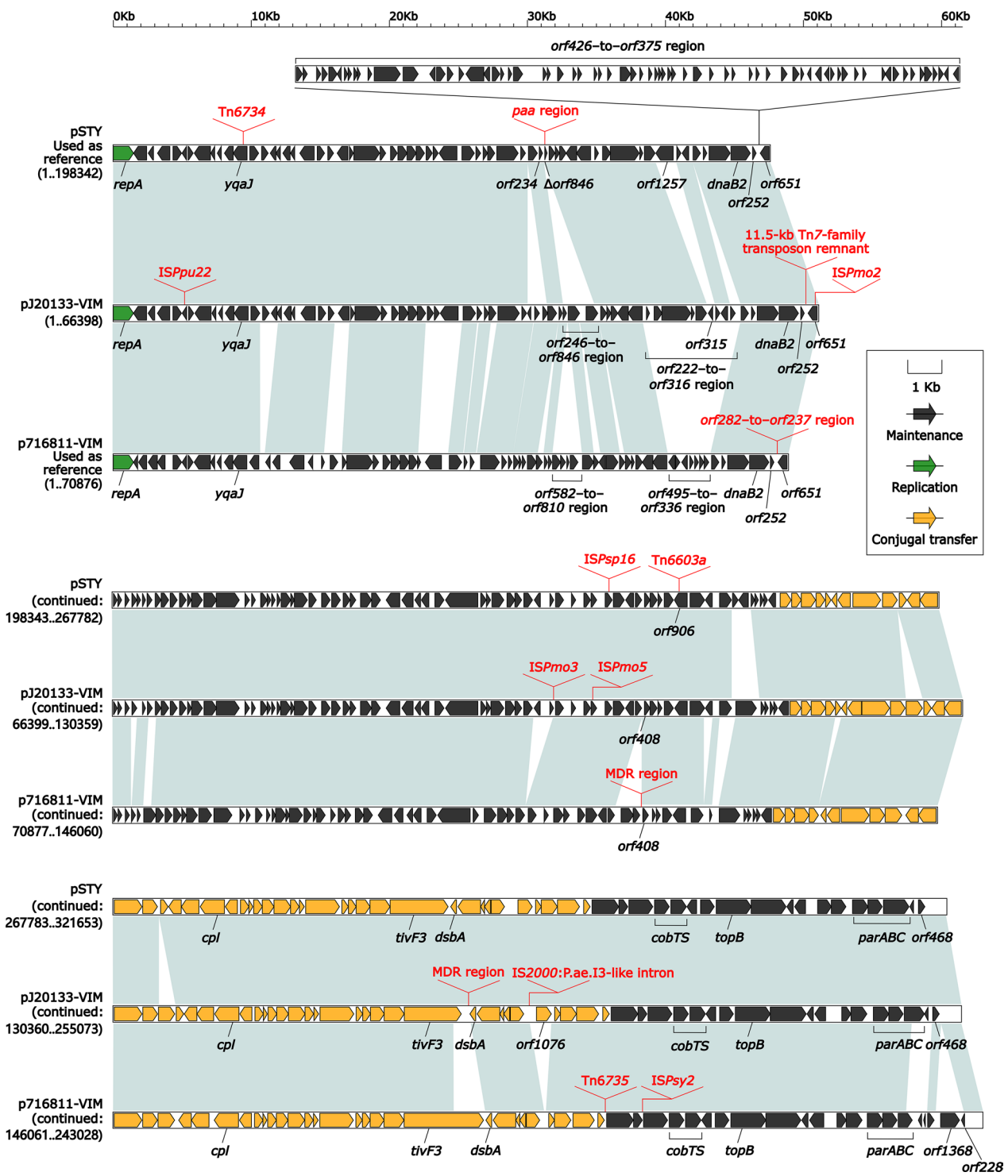


**Fig. 2** Linear comparison of the three $Inc_{pSTY}$ plasmids pSTY, pJ20133-VIM, and p716811-VIM. Genes are denoted by arrows. Genes, mobile elements and other features are colored based on function classification. Light blue shading regions denote nucleotide identity > 80%. Red characters represent accessory modules. Numbers in brackets indicate nucleotide positions within corresponding plasmids

could be divided into three separately clustering subgroups $Inc_{pSTY}$-1/2/3. As shown by pairwise comparison of *repA* sequences, plasmids within each subgroup showed ≥ 95% identity, while those from different subgroups displayed ≤ 95% but ≥ 82% identity (Additional file 1: Table S3). pSTY [28], p716811-VIM, and pHN39-SIM [10] were the first sequenced plasmids of $Inc_{pSTY}$-1, $Inc_{pSTY}$-2, and $Inc_{pSTY}$-3, respectively, and thus were identified as the references of the corresponding $Inc_{pSTY}$ subgroups.

### Comparison of three $Inc_{pSTY}$ plasmids pSTY, pJ20133-VIM and p716811-VIM

A detailed comparative genomics analysis was applied to three representative $Inc_{pSTY}$ plasmids including the $Inc_{pSTY}$-1 plasmids pSTY and pJ20133-VIM and the $Inc_{pSTY}$-2 plasmid p716811-VIM. The $Inc_{pSTY}$-3 plasmid pHN39-SIM was not included herein because it had been detailed characterized in our previous study [10]. These three characterized plasmids varied in size from about 243 to 321 kb with predicted ORFs from 255 to 282 (Table 1). The modular structure of each plasmid was divided into the backbone, and the accessory modules that were acquired DNA regions and inserted at different sites of the backbone (Fig. 2). pSTY, pJ20133-VIM, and p716811-VIM had > 80% nucleotide identity across > 66% of their backbone sequences, while pSTY and pJ20133-VIM shared > 74% of their backbones with > 95% nucleotide identity (Additional file 1: Table S4). These three plasmids shared the key $Inc_{pSTY}$ backbone markers: *repA* together with its iterons, *parABC* for partition, and multiple conjugal transfer genes (Fig. 2). A 47.9-kb backbone region *orf426*–to–*orf375* was presented in pSTY, but it was deleted from pJ20133-VIM and p716811-VIM due to insertion of an 11.5-kb Tn*7*-family transposon remnant (see below) and a 21.6-kb *orf282*–to–*orf237* region, respectively, at the same backbone site. The *orf282* – to – *orf237* region carried IS*1491*, *mvaT* (DNA-binding domain of bacterial xenogeneic silencer MvaT), five unnamed genes (encoding nucleoid-associated protein, predicted NTPase, AAA family ATPase, endonuclease, and putative transposase, respectively), and eight genes encoding hypothetical proteins.

pSTY, pJ20133-VIM, and p716811-VIM had totally different profiles of accessory modules (Table 1 and Fig. 2): (i) a 59.7-kb *paa* (phenylacetic acid degradation) region carrying *paa* locus and *mer* (mercury resistance) locus, Tn*6734*, Tn*6603a*, and IS*Psp16* in pSTY; (ii) a 67.2-kb MDR (multi-drug resistance) region, the 11.5-kb Tn*7*-family transposon remnant, IS*2000*:P.ae.I3-like intron, IS*Pmo2*, IS*Ppu22*, IS*Pmo3*, and IS*Pmo5* in pJ20133-VIM; and (iii) a 29.6-kb MDR region, Tn*6735*, *orf282*–to–*orf237* region, IS*1491*, and IS*Psy2* in p716811-VIM.

The integration of the 59.7-kb *paa* region into pSTY led to truncation of *orf246*–to–*orf846* region (as originally observed in pJ20133-VIM) into a 138-bp *orf846* remnant (Fig. 2). A presumed prototype *paa* region was terminally bracketed by two copies of Tn*5563* [29]; the right copy was intact while the left copy was truncated due to insertion of Tn*6481* in the 59.7-kb *paa* region from pSTY (Additional file 1: Fig. S1). This 59.7-kb *paa* region still contained a complete set of phenylacetic acid degradation genes (Additional file 1: Fig. S1). Tn*6734* was an IME containing a phenol degradation gene locus (Additional file 1: Fig. S2a). Tn*6603a* was a Tn*3*-family unit transposon containing an oxidative stress defense gene *osmC* (Additional file 1: Fig. S2b). The 67.2-kb MDR

**Table 1** Major features of the three $Inc_{pSTY}$ plasmids analyzed

| Plasmid | Accession number | Total length (bp) | Total number of ORFs | Mean G + C content (%) | Length of backbone (bp) | Accessory modules | | $bla_{VIM}$ | Host bacterium |
|---|---|---|---|---|---|---|---|---|---|
| | | | | | | Resistance | Non-resistance | | |
| pSTY | CP003962 | 321,653 | 355 | 56.8 | 210,612 | *paa* region | IS*Psp16*, Tn*6734*, and Tn*6603a* | None | *Pseudomonas taiwanensis* VLB120 |
| pJ20133-VIM | MN310371 | 255,073 | 298 | 56.5 | 168,325 | MDR region | IS*Ppu22*, IS*Pmo2*, IS*Pmo3*, IS*Pmo5*, IS*2000*:P.ae.I3-like intron, and 11.5-kb Tn*7*-family transposon remnant | $bla_{VIM-2}$ | *P. monteilii* J20133 |
| p716811-VIM | MN310372 | 243,028 | 262 | 55.4 | 163,184 | MDR region | IS*Psy2*, *orf282* – to – *orf237* region, and Tn*6735* | $bla_{VIM-2}$ | *P. putida* 716,811 |

The $Inc_{pSTY}$-1 reference plasmid pSTY [28] from GenBank, and the $Inc_{pSTY}$-1 plasmid pJ20133-VIM plus the $Inc_{pSTY}$-2 reference plasmid p716811-VIM sequenced in this study were included in a detailed sequence comparison

region from pJ20133-VIM contained In58, Tn*5046* and ΔTn*512*, a 3.6-kb Tn*4662a* remnant, and several IS elements (Additional file 1: Fig. S3).

According to the previous grouping scheme of Tn*7*-family transposons [30], the phylogenetic tree was constructed based on the nucleotide sequences of *tnsA*, which encoded the endonuclease responsible for excision of Tn*7*-family transposons. A phylogenetic analysis of Tn*6735*, the 11.5-kb Tn*7*-family transposon remnant, Tn*6922*, and Tn*6921*, together with additional 12 representative sequenced Tn*7*-family transposons from GenBank based on the *tnsA* genes, indicated that the first two belonged to a novel Tn*6735* subfamily and an unnamable subfamily (it had no intact sequenced transposon), respectively (Fig. 3). Similar to Tn*7* [31], both Tn*6735* (carrying pyrimidine biosynthesis genes) and the 11.5-kb Tn*7*-family transposon remnant encoded the core transposition determinants (endonuclease TnsA, transposase TnsB, regulator TnsC, target-site selection protein TnsD, and TnsB-binding sites), and the later one still encoded an additional target-site selection protein TnsE (Additional file 1: Fig. S4).

The 29.6-kb MDR region from p716811-VIM has a primary structure of a P.p.I3-like intron with interruption by Tn*6740* that carried $bla_{VIM-2}$, *aacA4*, *qnrVC1*, and *mer* locus (Additional file 1: Fig. S5). As a derivant of the IS*66*-family transposon Tn*5042* [32], Tn*6740* retained the whole Tn*5042* sequence with integration of a 21.2-kb region that comprised *mer*-containing Tn*3*-family unit transposon Tn*5563* [29], *qnrVC1*, and $bla_{VIM-2}$-carrying In1722 (see below) (Additional file 1: Fig. S5).

### Collection of 12 chromosome-borne IMEs/ICEs for sequence comparison

Three $bla_{VIM}$-carrying chromosomal MGEs Tn*6917*, Tn*6918* and Tn*6953* were identified from the complete genome sequences of the three *Pseudomonas* isolates 918607, 159349, and SE5443 (Additional file 1: Table S1). A detailed sequence comparison was applied to a total of 12 chromosomal MGEs belonging to three groups:

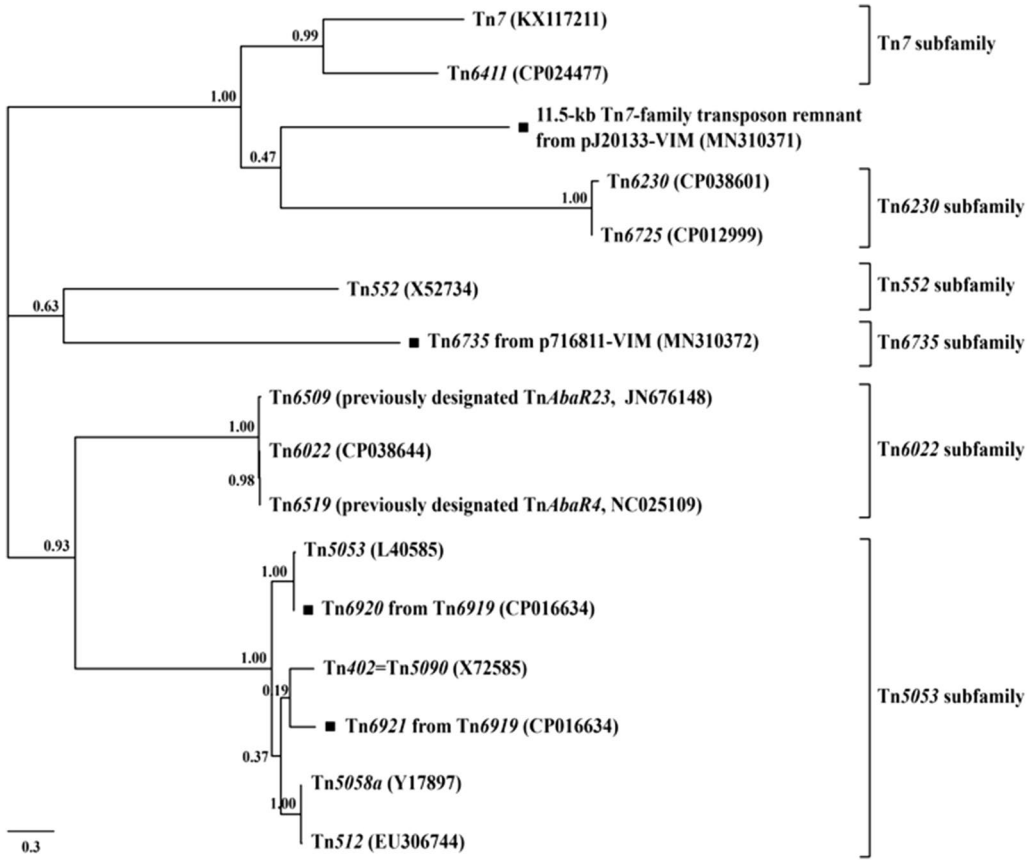


**Fig. 3** Evolutionary relationships of the Tn*7*-family transposons. A maximum likelihood phylogenetic tree was constructed from aligned *tnsA* sequences. Degree of support (percentage) for each cluster of associated taxa, as determined by bootstrap analysis, is shown next to each branch. Bar corresponds to scale of sequence divergence. Squares denote Tn*7*-family transposons or transposon remnants sequenced in this study

**Table 2** Major features of the 12 chromosome-borne IMEs and ICEs analyzed

| Category | MGE | Accession number | Host bacterium | Country | *bla*$_{VIM}$ | Nucleotide position in the chromosome | Refs. |
|---|---|---|---|---|---|---|---|
| Tn*6916*-related IMEs | Tn*6916* | CP014062 | *P. monteilii* FDAARGOS_171 | USA | None | Not applicable | [33] |
| | Tn*6917* | CP043395 | *P. monteilii* 918,607 | China | *bla*$_{VIM-2}$ | 2624899..2625699 | This study |
| Tn*6918*-related IMEs | Tn*6918* | CP045553 | *P. putida* 159,349 | China | *bla*$_{VIM-2}$ | 813783..814583 | This study |
| | Tn*6919* | CP016634 | *P. putida* IEC33019 | Brazil | None | Not applicable | — |
| Tn*6417*-related ICEs | Tn*6417* | CP013993 | *P. aeruginosa* DHS01 | France | None | Not applicable | [7] |
| | Tn*6413* | CP030075 | *P. aeruginosa* 6762 | China | *bla*$_{VIM-4}$ | 409196..409996 | [7] |
| | Tn*6953* | CP046405 | *P. aeruginosa* SE5443 | China | *bla*$_{VIM-2}$ | 4906548..4907348 | This study |
| | Tn*6954* | KY623658 | *Alcaligenes faecalis* GZAF3 | Palestine | *bla*$_{VIM-2}$ | 63643..64443 | [36] |
| | Tn*6955* | MF168944 | *P. aeruginosa* HSV3483 | Portugal | *bla*$_{VIM-2}$ | 62615..63415 | [3] |
| | Tn*6956* | MF168946 | *P. aeruginosa* FFUP_PS_CB5 | Portugal | *bla*$_{VIM-2}$ | 93931..94731 | [3] |
| | Tn*6957* | CP043328 | *P. aeruginosa* CCUG 51971 | Sweden | *bla*$_{VIM-4}$ | 5251865..5252665 | – |
| | Tn*6958* | CP048039 | *A. faecalis* MUB14 | Poland | *bla*$_{VIM-4}$ | 659107..659907 | [37] |

A collection of 12 fully sequenced chromosome-borne MGEs, which included all the four Tn*6916*- or Tn*6918*-related IMEs and the eight Tn*6417*-related ICEs composed of Tn*6417* itself plus all the six *bla*$_{VIM}$-carrying ones, were included in a detailed sequence comparison

two related IMEs Tn*6916* and Tn*6917*; two related IMEs Tn*6918* and Tn*6919*; and eight related ICEs Tn*6417*, Tn*6413*, Tn*6953*, Tn*6454*, Tn*6455*, Tn*6456*, Tn*6457* and Tn*6458* (Table 2; last accessed August 10th 2020). Tn*6917* was the only *bla*$_{VIM}$-carrying one belonging to Tn*6916*-related IMEs in GenBank. Tn*6919* was the only one (in addition to Tn*6918*) belonging to Tn*6918*-related IMEs in GenBank, and it did not carry *bla*$_{VIM}$. The seven Tn*6417*-related ICEs were selected from GenBank because Tn*6417* was used as reference and the rest six ones Tn*6413*, Tn*6954*, Tn*6955*, Tn*6956*, Tn*6957* and Tn*6958* carried *bla*$_{VIM}$ genes. Similar to the above Inc$_{pSTY}$ plasmids, the modular structure of each IME/ICE was divided into the backbone and the accessory modules.

#### Comparison of two related IMEs Tn*6916* and Tn*6917*

Tn*6916* (a 51.0-kb prototype IME initially identified in *P. monteilii* FDAARGOS_171 [33]) and Tn*6917* were integrated at the same site downstream of the *P. monteilii* chromosomal gene *dinG* (ATP-dependent DNA helicase), and they shared the core backbone markers *attL* (attachment site at the left end), *int* (integrase), and *attR* (attachment site at the right end); in addition, the β-lactam resistance gene *ampC* was considered as a backbone component of these two IMEs because no associated MGEs were identified for this resistance gene (Fig. 4). Tn*6916* thereby had no accessory modules, but *bla*$_{VIM-2}$-carrying In528 (see below) was integrated at a site upstream of *eamA* (transcription regulator) and identified as the sole accessory module in Tn*6917* (Fig. 4).

#### Comparison of two related IMEs Tn*6918* and Tn*6919*

Tn*6918* (a 70.49-kb prototype IME initially found in *P. putida* 159,349) and Tn*6919* were integrated at a site downstream of the *P. putida* chromosomal gene tRNA$^{Thr}$, and they shared the core backbone markers *attL*, *int1*, *int2*, and *attR* (Fig. 5). There were at least three major modular differences in the backbone of Tn*6919* relative to Tn*6918*: i) inversion of *orf1965*, ii) interruption of *orf549* and *orf2007* due to insertion of ΔIS*Ppu13* and IS*Pen2*, respectively, and iii) replacement of 3'-termimal 22.8-kb *orf270*–to–*orf213* region by 3.4-kb *orf255*–to–*orf282* region (Fig. 5). The IS*Pa122*–*mer* region was integrated at the same site of the backbones of Tn*6918* and Tn*6919* (Fig. 5), and it was composed of IS*Pa122* and a *mer*-carrying ΔTn*5041*-like element (Additional file 1: Fig. S6). Tn*6918* and Tn*6919* acquired *bla*$_{VIM-2}$-carrying In1770 (see below) and *strAB* region, respectively, which were inserted at the same site upstream of *orf555* (Fig. 5). The *strAB* region

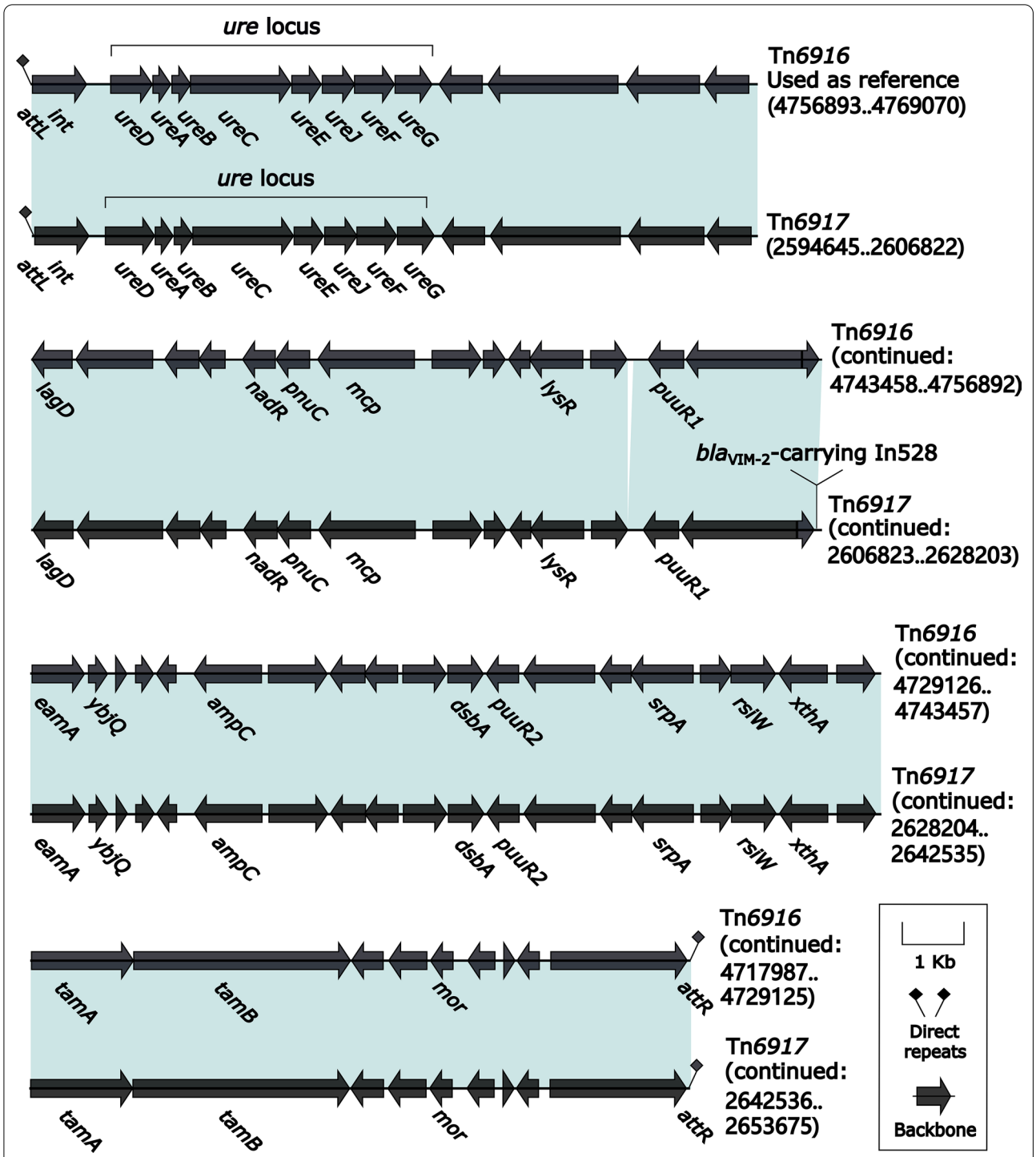


**Fig. 4** Comparison of the two-related IMEs Tn*6916* and Tn*6917*. Genes are denoted by arrows. Genes, mobile elements and other features are colored based on their functional classification. Shading regions denotes of nucleotide identity ≥ 95%. Numbers in brackets indicate nucleotide positions within the chromosomes of strains FDAARGOS_171 and 918607, respectively. The accession number of Tn*6916* [33] for reference is CP014062

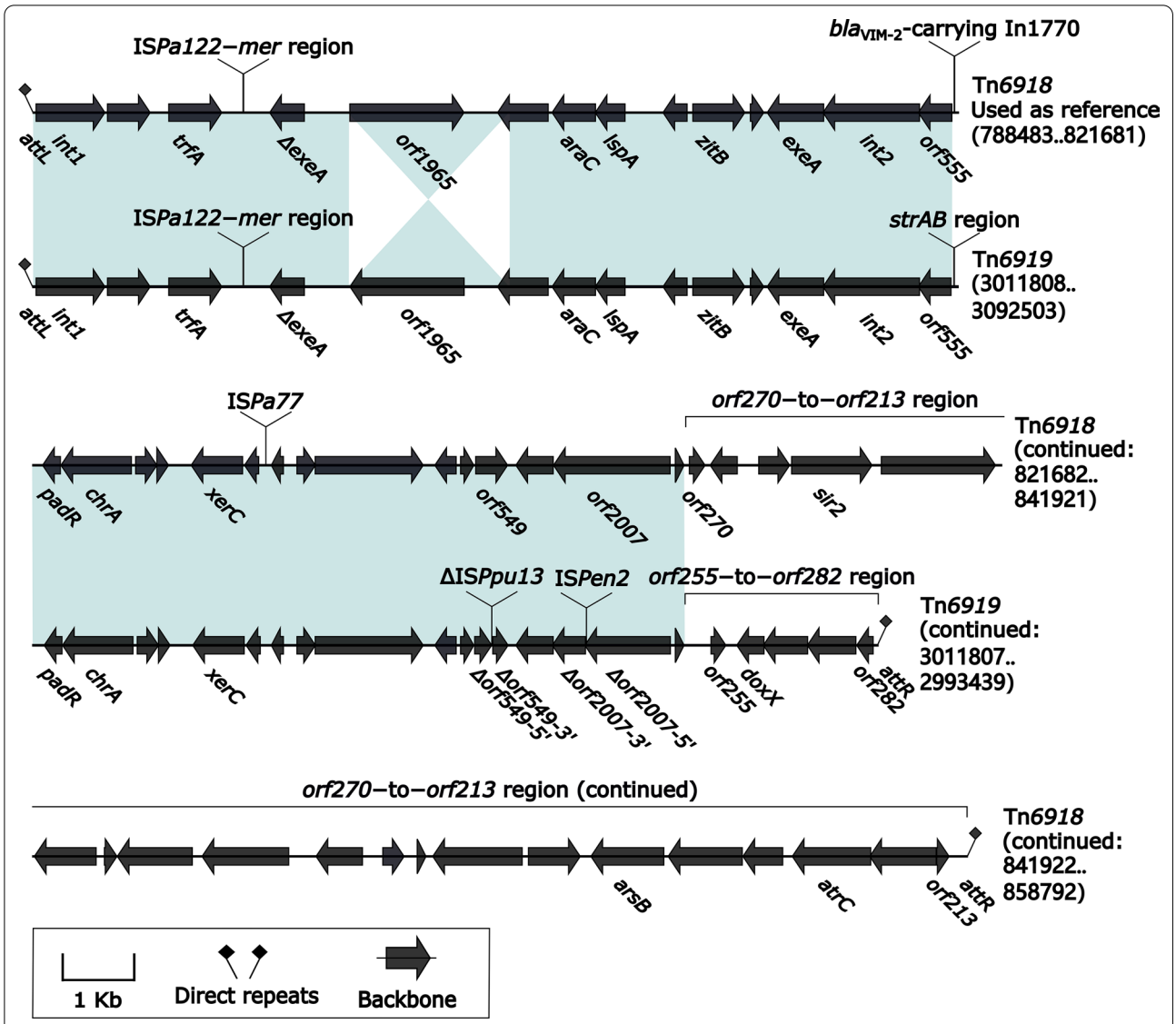


**Fig. 5** Comparison of the two-related IMEs Tn*6918* and Tn*6919*. Genes are denoted by arrows. Genes, mobile elements and other features are colored based on their functional classification. Shading regions denotes of nucleotide identity ≥ 95%. Numbers in brackets indicate nucleotide positions within the chromosomes of strains 159349 and IEC33019, respectively. The accession number of Tn*6918* for reference is CP045553

contained a cryptic unit transposon Tn*6920*, a *strAB*-carrying unit transposon Tn*6921*, a 3.6-kb Tn*4662a* remnant, and several IS elements (Additional file 1: Fig. S7). Tn*6920* and Tn*6921* had the core transposition *tniABQ*−*res*−*tniR* modules with the highest sequence identities to Tn*5053* [34] and Tn*5058a* [32], respectively, and thus they belonged to the Tn*5053* subfamily of Tn*7* family (Fig. 3).

#### Comparison of eight Tn*6417*-related ICEs

Tn*6417* was a 108.2-kb reference ICE [7] initially found in *P. aeruginosa* DHS01 [35]. The eight related ICEs Tn*6417*, Tn*6413*, Tn*6953*, Tn*6954* (GZAF3_GI) [36], Tn*6955* (ICE*6440*) [3], Tn*6956* (ICE*6441*) [3], Tn*6957*, and Tn*6958* [37] shared the core backbone markers *attL*/*attR* (these sequences showed somewhat differences but shared a core motif 'CCTTCGCCCGCTCCA'), *int*, *cpl* (coupling protein), *rlx* (relaxase), and a F (TivF)-type type IV secretion system gene set (mating pair formation). However, the backbones of these eight ICEs varied in size from 67.8 to 95.1 kb and had at least four major modular differences: (i) presence of unique *orf672*, *orf306*, *piL1*–to–*orf381* region, and *orf3336*–to–*orf2514* region in Tn*6953*; (ii) presence of two highly similar regions

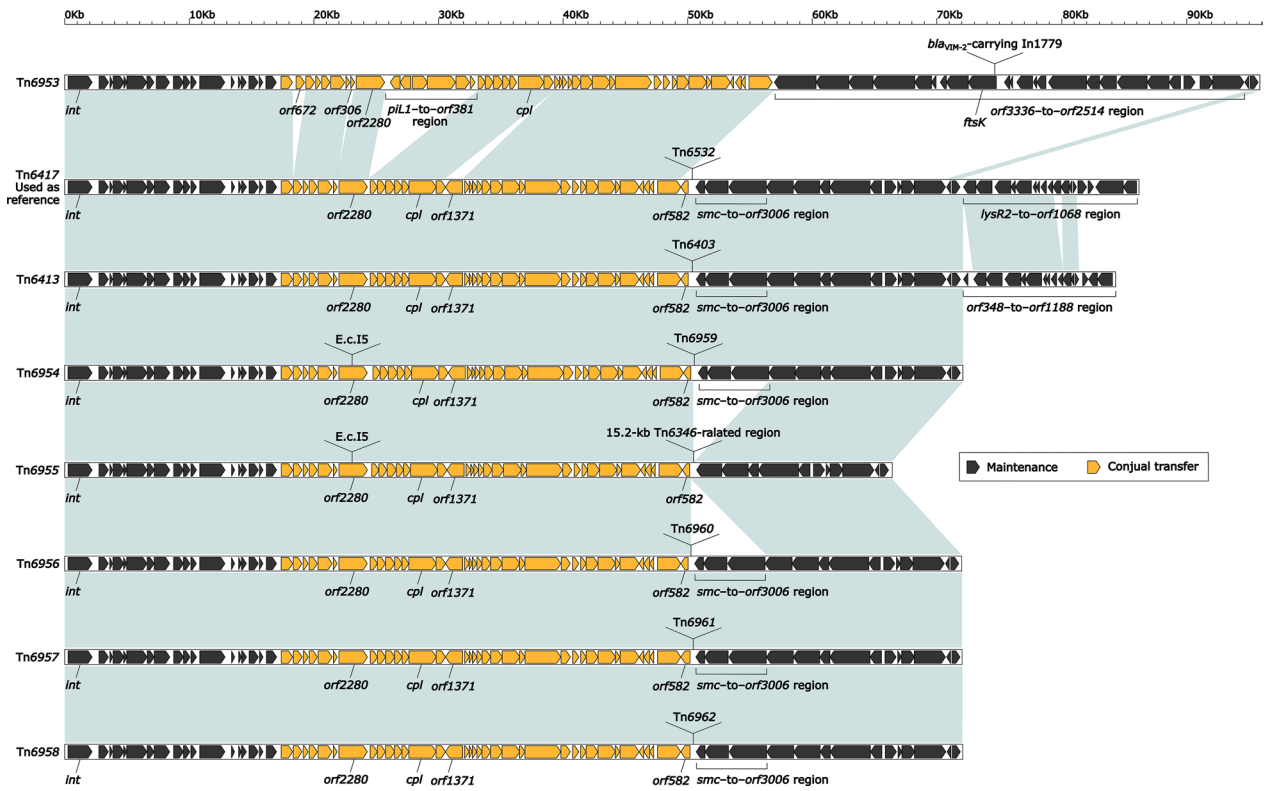


**Fig. 6** Comparison of Tn*6417* and the seven related ICEs. Genes are denoted by arrows. Genes, mobile elements and other features are colored based on their functional classification. Shading regions denote nucleotide identity ≥ 95%. Accession number of Tn*6417* [7] for reference is EU696790

*lysR2*–to–*orf1068* and *orf348*–to–*orf1188* in Tn*6417* and Tn*6413*, respectively; (iii) absence of *smc*–to–*orf3006* region from Tn*6955*; and (iv) interruption of *orf2280* owing to insertion of intron E.c.I5 in Tn*6954* and Tn*6955* (Fig. 6). The first six ICEs were integrated into the *P. aeruginosa* or *A. faecalis* chromosomal $tRNA^{Gly}$ gene, while the last two ones into the *P. aeruginosa* chromosomal gene *mhpC* (methyl ester carboxylesterase) and *orf1203* (putative DNA-binding protein), respectively.

Each ICE carried a single accessory module, and thus there were the resulting eight different accessory modules $bla_{VIM-2}$-carrying In1779 (see below), Tn*6532*, Tn*6403*, Tn*6959*, a 15.2-kb Tn*6346*-related region, Tn*6960*, Tn*6961*, and Tn*6962* from the eight ICEs; the first one was inserted into *ftsk* (cell division protein), while all the other seven ones were integrated at a site upstream of *orf582* and identified as the derivatives of Tn*6346* (Fig. 7). Tn*6346* was a prototype Tn*3*-family unit transposon originally identified in *Achromobacter* spp. AO22 [38] and manifested as a hybrid of the core transposition module *tnpAR–res* from Tn*5051* and the *mer* region from Tn*501* (Fig. 7). The seven Tn*6346* derivatives differed from Tn*6346* in two major aspects: (i) insertion of IS*1071* at the same position within *tnpA* in all these seven Tn*6346* derivatives, and furthermore insertion of IS*Pa91* at another position within *tnpA* in only Tn*6960*; and (ii) insertion of different concise class 1 integrons In159, In127, In1365, In56, In1879, In1853, and In58

(See figure on next page.)

**Fig. 7** Comparison of Tn*6346* and the seven related elements. Genes are denoted by arrows. Genes, mobile elements and other features are colored based on their functional classification. Shading regions denote nucleotide identity (light blue: ≥95%; and light pink: <95% but ≥ 79%). Numbers in brackets indicate nucleotide positions within the chromosomes of strains DHS01, 6762, GZAF3, FFUP_PS_CB5, CCUG 51971, MUB14, and HSV3483, respectively. The accession number of Tn*6346* [38] for reference is EU696790

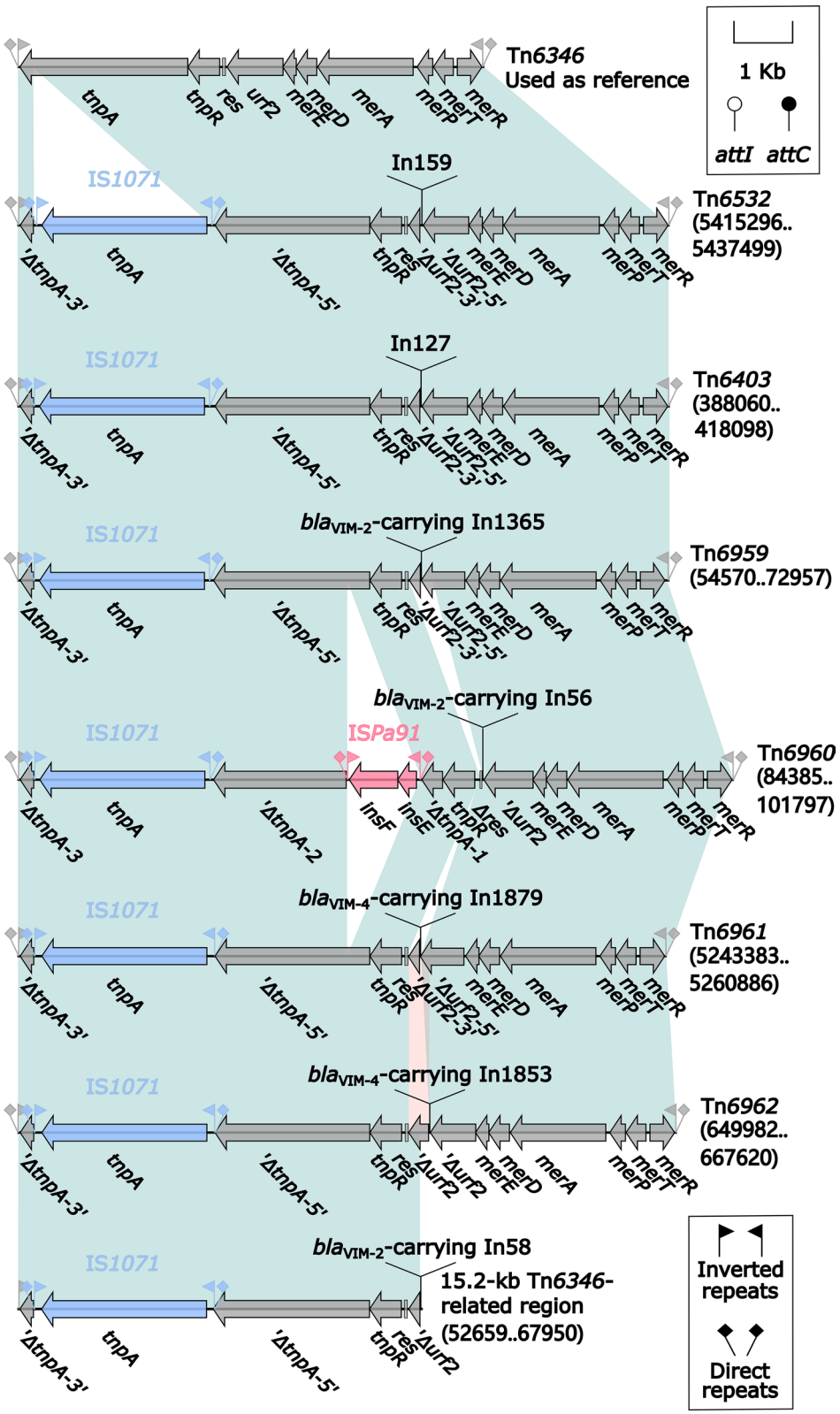


**Fig. 7** (See legend on previous page.)

into *urf2* in these seven Tn*6346* derivatives, sometimes leading to truncation of surrounding regions (Fig. 7). The $bla_{VIM}$ genes were found the last five integrons (see below) rather than the first two (Additional file 1: Fig. S8).

#### Comparison of eleven $bla_{VIM}$-carrying integrons

The $bla_{VIM}$ genes were found in the two plasmids pJ20133-VIM and p716811-VIM (Table 1) and the nine chromosomal IMEs/ICEs Tn*6917*, Tn*6918*, Tn*6413*, Tn*6953*, Tn*6454*, Tn*6455*, Tn*6456*, Tn*6457* and Tn*6458* (Table 2). The 11 corresponding local $bla_{VIM}$ genetic environments manifested as 11 different class 1 concise integrons, and three of them contained $bla_{VIM-4}$ while the other nine carried $bla_{VIM-2}$ (Fig. 8). A complete class 1 concise integron contained IRi (inverted repeat at the integrase end), 5'-conserved segment (5'-CS: *intI1–attI1*), GCA, 3'-CS (*qacED1–sul1–orf5–orf6*), $tni_{Tn402}$ (Tn*402* core transposition module *tniABQ–res–tniR*), and IRt (inverted repeat at the *tni* end). Except for $In1443_{Tn6413}$ with terminal truncations, all the other tens had the terminal IRi/IRt pairs. Insertions or truncations occurred in 5'-CS or 3'-CS or $tni_{Tn402}$ of all these 11 integrons, especially including In1779 that showed the longest modular structure because of integration of a *mer*-containing Tn*3*-family prototype unit transposon Tn*6758*. $In56_{Tn6596}$ had the shortest GCA that contained only $bla_{VIM-2}$, while all the other 10 integrons had the multiple-gene GCAs harboring $bla_{VIM-2}$ plus one or more additional antibiotic resistance genes.

#### Summary of newly identified or designated MGEs

There were eight newly identified MGEs, including two IMEs Tn*6917* and Tn*6918*, one ICE Tn*6953*, two unit transposons Tn*6735* and Tn*6740*, and three integrons In1770, In1772, and In1779. Additional 13 MGEs (IMEs: Tn*6734*, Tn*6916*, Tn*6919*, and Tn*6957*; unit transposons: Tn*6920*, Tn*6921*, Tn*6959*, Tn*6960*, Tn*6961*, and Tn*6962*; IS elements: IS*Pmo2*, IS*Pmo3*, IS*Pmo5*) were newly designated but with previously determined sequences. The three previously designated ICEs GZAF3_GI, ICE*6440*, and ICE*6441* were renamed as the standard Tn designations Tn*6954*, Tn*6955*, and Tn*6956*, respectively.

#### Transferability and antimicrobial susceptibility

pJ20133-VIM, p716811-VIM, and Tn*6953*, which were selected to represent the $Inc_{pSTY}$-1 and $Inc_{pSTY}$-2 plasmids and the Tn*6417*-related ICEs, respectively, could be transferred from the relevant wild-type isolates into ATCC 27853 or PAO1 through conjugation, generating the transconjugants PAO1/pJ20133-VIM, PAO1/p716811-VIM, and ATCC 27853/Tn*6953* respectively. All these wild-type and transconjugant strains had the Ambler class B carbapenemase activity (data not shown) and were resistant to imipenem and meropenem with minimal inhibit concentration (MIC) values ≥ 16 mg/L (Additional file 1: Table S5), owing to production of VIM enzyme.

## Discussion

The present work identifies a novel group of $Inc_{pSTY}$ plasmids, which can be further divided into the three subgroups $Inc_{pSTY}$-1/2/3. A detailed genetic dissection analysis is applied to a collection of 15 *Pseudomonas* MGEs, including three $Inc_{pSTY}$ plasmids, two Tn*6916*-related IMEs, two Tn*6918*-related IMEs, and eight Tn*6417*-related ICEs. All these IMEs/ICEs were located within the bacterial chromosomes. At least 22 genes for resistance to seven different categories of antibiotics and heavy metals are identified within these 15 MGEs (Additional file 1: Table S6). Eleven of these 15 MGEs carry the $bla_{VIM}$ genes, which are all located within GCAs of concise class 1 integrons. For 10 of these integrons, the $bla_{VIM}$ genes were presented together with other resistance genes, especially including those for resistance to β-lactams, aminoglycosides, trimethoprim, and rifampicin. These $bla_{VIM}$-carrying integrons were further integrated into the above plasmids, IMEs and ICEs.

Confirmed by conjugal transfer experiments herein, $Inc_{pSTY}$ plasmids and Tn*6417*-related ICEs have the ability to transfer from one cell to another cell. These two groups MGEs could transfer autonomously by utilizing self-encoded conjugation gene sets [39, 40]. However, the conjugal transfer of Tn*6916*- and Tn*6918*-related IMEs are nonautonomous due to lack of essential conjugation genes encoding Cpl and type IV secretion system, and thereby its intercellular transfer is relied on the help of other conjugative elements [40].

$bla_{VIM}$ genes are widely disseminated in *Pseudomonas* [41–43], Enterobacteriaceae [5, 44, 45], *Providencia* [46, 47], *Achromobacter* [48], *Acinetobacter* [49, 50], *Aeromonas* [51], and *Morganella* [52]. Currently, at least 183 different $bla_{VIM}$-carrying integrons [19, 53, 54] have been identified, and they either directly integrate into the chromosomes or reside as the inner-components of various MGEs such as plasmids, unit transposons, ICEs and IMEs [3, 55–57].

(See figure on next page.)

**Fig. 8** Comparison of the 11 $bla_{VIM}$-carrying integrons. Genes are denoted by arrows. Genes, mobile elements and other features are colored based on their functional classification. Shading regions denote of nucleotide identity (light blue and yellow: ≥ 95%; and light pink <95% but ≥ 85%). Numbers in brackets indicate nucleotide positions within the corresponding plasmids pJ20133-VIM and p716811-VIM or within the chromosomes of strains FFUP_PS_CB5, 6762, GZAF3, HSV3483, CCUG 51971, MUB14, 159349, 918607, and SE5443

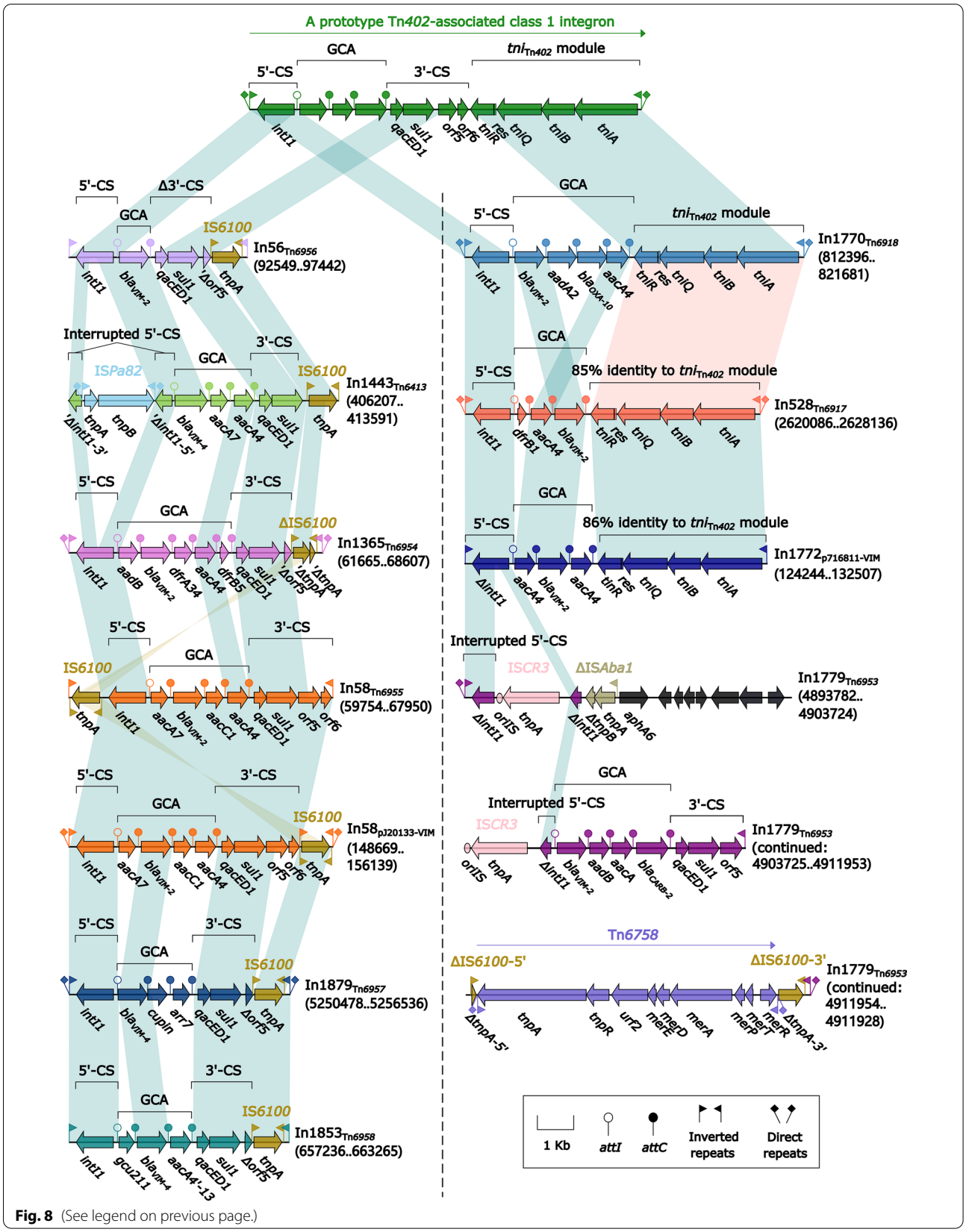


**Fig. 8** (See legend on previous page.)

These results indicate that $bla_{VIM}$ genes have evolved to reside diverse MGEs with the intra- or inter-cellular mobility, which will promote the wide dissemination of $bla_{VIM}$ genes.

Until now, only seven $Inc_{pSTY}$ plasmids are identified in six *Pseudomonas* isolates and one *Stenotrophomonas rhizophila* isolate, which come from China (n = 5), Japan (n = 1) and Germany (n = 1) (Additional file 1: Table S2). Only six Tn*6916*-related IMEs and two Tn*6918*-related IMEs are detected in eight *Pseudomonas* isolates, two of which are sequenced in this study. The six Tn*6916*-related IMEs come from China (n = 4), USA (n = 1) and Japan (n = 1), while the two Tn*6918*-related IMEs from China (n = 1) and Brazil (n = 1). These observations indicate that these three group MGEs are mainly prevalent in *Pseudomonas* isolates and meanwhile still not widely disseminated in multiple geographic regions. By contrast, Tn*6417*-related ICEs are frequently identified in *Pseudomonas* [7, 58, 59] and also occasionally in *Bordetella*, *Alcaligenes*, *Klebsiella pneumoniae*, *Achromobacter xylosoxidans*, *Morganella morganii*, *Aeromonas caviae*, *Casimicrobium huifangae*, and *Delftia acidovorans*. Tn*6417*-related ICEs have been already disseminated worldwide in a plenty of bacterial species.

## Conclusion

The four groups of $bla_{VIM}$-carrying MGEs characterized in this study have a wide range of hosts including *Pseudomonas*, and they are able to transfer across different bacterial species. Integration of $bla_{VIM}$ genes into these MGEs contributes to the accumulation and distribution of $bla_{VIM}$ genes and enhances the ability of bacteria to survive under selection pressure of carbapenems especially in hospital settings. Moreover, these four groups of MGEs display a high-level diversification in modular structures, which have complex mosaic natures and carry a large number of drug resistance genes (particularly in the MDR regions in these MGEs). This study provides a deeper insight into the genetic diversification and evolution of VIM-encoding MGEs in *Pseudomonas*.

#### Abbreviations

MGE: Mobile genetic element; ICE: Integrative and conjugative element; IME: Integrative and mobilizable element; GCA: Gene cassette array; Inc: Incompatibility; RAST: Rapid Annotation using Subsystem Technology; BHI: Brain Heart Infusion; CLSI: Clinical and Laboratory Standards Institute; MLST: Multi-locus Sequence Typing; MDR: Multi-drug resistance; IRi: Inverted repeat at the integrase end; CS: Conserved segment; IRt: Inverted repeat at the *tni* end; MIC: Minimal inhibit concentration.

## Supplementary Information

The online version contains supplementary material available at https://doi.org/10.1186/s12941-022-00502-w.

**Additional file 1: Fig S1.** Organization of *paa* region from pSTY. **Fig S2.** Organization of Tn*6734* and Tn*6603a* from pSTY. **Fig S3.** Organization of MDR region from pJ20133-VIM, and comparison with related regions. **Fig S4.** Organization of two Tn*7*-family elements, and comparison with related region. **Fig S5.** Organization of MDR region from p716811-VIM, and comparison with related regions. **Fig S6.** Organization of IS*Pa122*—*mer* region from Tn*6918* and Tn*6919*, and comparison with related region. **Fig S7.** Organization of *strAB* region from Tn*6919*, and comparison with related regions. **Fig S8.** Organization of In159 and In127 from Tn*6532* and Tn*6403* respectively, and comparison with related region. **Table S1.** Major features of the five *Pseudomonas* isolates sequenced in this study. **Table S2.** List of all the seven sequenced $Inc_{pSTY}$ single-replicon plasmids. **Table S3.** Pairwise comparison of $repA_{IncpSTY}$ sequences from the seven $Inc_{pSTY}$ plasmids using BLASTN. **Table S4.** Pairwise comparison of backbone sequences from the three $Inc_{pSTY}$ plasmids using BLASTN. **Table S5.** Antimicrobial drug susceptibility profiles. **Table S6.** Resistance genes in the 15 mobile genetic elements (MGEs) analyzed.

#### Acknowledgements

Not applicable.

#### Authors' contributions

DZ and JW conceived the study and designed experimental procedures. FC, HY, LH and TY performed the experiments. FC, JJ, and JG analyzed the data. ZY and PW contributed to reagents and materials. FC and HY wrote the original draft. DZ and JW reviewed the manuscript. All authors read and approved the final manuscript.

#### Funding

This work was supported by the National Natural Science Foundation of China (Grant No. 3214100027).

#### Availability of data and materials

The complete sequences of plasmids pJ20133-VIM and p716811-VIM, and those of the chromosomes of strains SE5443, 918607, and 159349 were submitted to GenBank under accession numbers MN310371, MN310372, CP046405, CP043395, and CP045553 respectively.

## Declarations

#### Ethics approval and consent to participate

Not applicable.

#### Consent for publication

Not applicable.

#### Competing interests

The authors declare that they have no competing interests.

#### Author details

[1]State Key Laboratory of Pathogen and Biosecurity, Beijing Institute of Microbiology and Epidemiology, Beijing 100071, China. [2]Basic Medical College, Guizhou Medical University, Guiyang 550025, China. [3]Guangzhou Medical University, Guangzhou 511436, China.

Received: 6 April 2021 Accepted: 2 March 2022
Published online: 09 March 2022

#### References

1. Queenan AM, Bush K. Carbapenemases: the versatile beta-lactamases. Clin Microbiol Rev. 2007;20:440–58.
2. Toleman MA, Vinodh H, Sekar U, et al. $bla_{VIM-2}$-harboring integrons isolated in India, Russia, and the United States arise from an ancestral class 1 integron predating the formation of the 3′conserved sequence. Antimicrob Agents Chemother. 2007;51:2636–8.

3. Botelho J, Grosso F, Quinteira S, et al. Two decades of $bla_{VIM-2}$-producing *Pseudomonas aeruginosa* dissemination: an interplay between mobile genetic elements and successful clones. J Antimicrob Chemother. 2018;73:873–82.
4. Gaibani P, Ambretti S, Scaltriti E, et al. A novel IncA plasmid carrying $bla_{VIM-1}$ in a *Kluyvera cryocrescens* strain. J Antimicrob Chemother. 2018;73:3206–8.
5. Miriagou V, Papagiannitsis CC, Kotsakis SD, et al. Sequence of pNL194, a 79.3-kilobase IncN plasmid carrying the blaVIM-1 metallo-beta-lactamase gene in Klebsiella pneumoniae. Antimicrob Agents Chemother. 2010;54:4497–502.
6. Peirano G, Lascols C, Hackel M, et al. Molecular epidemiology of *Enterobacteriaceae* that produce VIMs and IMPs from the SMART surveillance program. Diagn Microbiol Infect Dis. 2014;78:277–81.
7. Zeng L, Zhan Z, Hu L, et al. Genetic characterization of a $bla_{VIM-24}$-carrying IncP-7β plasmid p1160-VIM and a $bla_{VIM-4}$-harboring integrative and conjugative element Tn*6413* from clinical *Pseudomonas aeruginosa*. Front Microbiol. 2019;10:213.
8. Botelho J, Schulenburg H. The role of integrative and conjugative elements in antibiotic resistance evolution. Trends Microbiol. 2021;29:8–18.
9. Guedon G, Libante V, Coluzzi C, et al. The obscure world of integrative and mobilizable elements, highly widespread elements that pirate bacterial conjugative systems. Genes (Basel). 2017;8:337.
10. Sun F, Zhou D, Wang Q, et al. The first report of detecting the $bla_{SIM-2}$ gene and determining the complete sequence of the SIM-encoding plasmid. Clin Microbiol Infect. 2016;22:347–51.
11. Fu J, Zhang J, Yang L, et al. Precision methylome and in vivo methylation kinetics characterization of *Klebsiella pneumoniae*. GPB. 2021. https://doi.org/10.1016/j.gpb.2021.04.002.
12. Hackl T, Hedrich R, Schultz J, et al. Proovread: large-scale high-accuracy PacBio correction through iterative short read consensus. Bioinformatics. 2014;30:3004–11.
13. Brettin T, Davis JJ, Disz T, et al. RASTtk: a modular and extensible implementation of the RAST algorithm for building custom annotation pipelines and annotating batches of genomes. Sci Rep. 2015;5:8365.
14. Boratyn GM, Camacho C, Cooper PS, et al. BLAST: a more efficient report with usability improvements. Nucleic Acids Res. 2013;41:W29-33.
15. O'Leary NA, Wright MW, Brister JR, et al. Reference sequence (RefSeq) database at NCBI: current status, taxonomic expansion, and functional annotation. Nucleic Acids Res. 2016;44:D733–45.
16. Jia B, Raphenya AR, Alcock B, et al. CARD 2017: expansion and model-centric curation of the comprehensive antibiotic resistance database. Nucleic Acids Res. 2017;45:D566–73.
17. Zankari E, Hasman H, Cosentino S, et al. Identification of acquired antimicrobial resistance genes. J Antimicrob Chemother. 2012;67:2640–4.
18. Siguier P, Perochon J, Lestrade L, et al. ISfinder: the reference centre for bacterial insertion sequences. Nucleic Acids Res. 2006;34:D32–6.
19. Moura A, Soares M, Pereira C, et al. INTEGRALL: a database and search engine for integrons, integrases and gene cassettes. Bioinformatics. 2009;25:1096–8.
20. Roberts AP, Chandler M, Courvalin P, et al. Revised nomenclature for transposable genetic elements. Plasmid. 2008;60:167–73.
21. Sievers F, Higgins DG. Clustal Omega for making accurate alignments of many protein sequences. Protein Sci. 2018;27:135–45.
22. Kumar S, Stecher G, Li M, et al. MEGA X: molecular evolutionary genetics analysis across computing platforms. Mol Biol Evol. 2018;35:1547–9.
23. CLSI. Performance standards for antimicrobial susceptibility testing. Wayne: Clinical and Laboratory Standards Institute; 2020.
24. Sun F, Yin Z, Feng J, et al. Production of plasmid-encoding NDM-1 in clinical *Raoultella ornithinolytica* and *Leclercia adecarboxylata* from China. Front Microbiol. 2015;6:458.
25. Carloni E, Andreoni F, Omiccioli E, et al. Comparative analysis of the standard PCR-Based Replicon Typing (PBRT) with the commercial PBRT-KIT. Plasmid. 2017;90:10–4.
26. Carattoli A, Bertini A, Villa L, et al. Identification of plasmids by PCR-based replicon typing. J Microbiol Methods. 2005;63:219–28.
27. Partridge SR, Kwong SM, Firth N, et al. Mobile genetic elements associated with antimicrobial resistance. Clin Microbiol Rev. 2018. https://doi.org/10.1128/CMR.00088-17.
28. Kohler KA, Ruckert C, Schatschneider S, et al. Complete genome sequence of *Pseudomonas* sp. strain VLB120 a solvent tolerant, styrene degrading bacterium, isolated from forest soil. J Biotechnol. 2013;168:729–30.
29. Yeo CC, Tham JM, Kwong SM, et al. Tn*5563*, a transposon encoding putative mercuric ion transport proteins located on plasmid pRA2 of *Pseudomonas alcaligenes*. FEMS Microbiol Lett. 1998;165:253–60.
30. Peters JE, Fricker AD, Kapili BJ, et al. Heteromeric transposase elements: generators of genomic islands across diverse bacteria. Mol Microbiol. 2014;93:1084–92.
31. Peters JE, Craig NL. Tn*7*: smarter than we thought. Nat Rev Mol Cell Biol. 2001;2:806–14.
32. Mindlin S, Minakhin L, Petrova M, et al. Present-day mercury resistance transposons are common in bacteria preserved in permafrost grounds since the Upper Pleistocene. Res Microbiol. 2005;156:994–1004.
33. Sichtig H, Minogue T, Yan Y, et al. FDA-ARGOS is a database with public quality-controlled reference genomes for diagnostic use and regulatory science. Nat Commun. 2019;10:3313.
34. Kholodii GY, Yurieva OV, Lomovskaya OL, et al. Tn*5053*, a mercury resistance transposon with integron's ends. J Mol Biol. 1993;230:1103–7.
35. Valot B, Rohmer L, Jacobs MA, et al. Comparative genomic analysis of two multidrug-resistant clinical isolates of ST395 epidemic strain of *Pseudomonas aeruginosa* obtained 12 years apart. Genome Announc. 2014;2:e00515-e614.
36. Al Laham N, Chavda KD, Cienfuegos-Gallet AV, et al. Genomic characterization of VIM metallo-β-Lactamase-producing *Alcaligenes faecalis* from Gaza. Palestine Antimicrob Agents Chemother. 2017;61:e01499-e1517.
37. Majewski P, Majewska P, Gutowska A, et al. Molecular characterisation of clinical pandrug-resistant *Alcaligenes faecalis* strain MUB14. Int J Antimicrob Agents. 2020;55:105939.
38. Ng SP, Davis B, Palombo EA, et al. A Tn5051-like mer-containing transposon identified in a heavy metal tolerant strain *Achromobacter* sp. AO22. BMC Res Notes. 2009;2:38.
39. Smillie C, Garcillán-Barcia MP, Francia MV, et al. Mobility of plasmids. Microbiol Mol Biol Rev. 2010;74:434–52.
40. Bellanger X, Payot S, Leblond-Bourget N, et al. Conjugative and mobilizable genomic islands in bacteria: evolution and diversity. FEMS Microbiol Rev. 2014;38:720–60.
41. Li R, Peng K, Xiao X, et al. Emergence of a multidrug resistance efflux pump with carbapenem resistance gene blaVIM-2 in a Pseudomonas putida megaplasmid of migratory bird origin. J Antimicrob Chemother. 2021;76:1455–8.
42. Hishinuma T, Uchida H, Tohya M, et al. Emergence and spread of VIM-type metallo-β-lactamase-producing *Pseudomonas aeruginosa* clinical isolates in Japan. J Glob Antimicrob Resist. 2020;23:265–8.
43. Ocampo-Sosa AA, Guzmán-Gómez LP, Fernández-Martínez M, et al. Isolation of VIM-2-producing *Pseudomonas monteilii* clinical strains disseminated in a tertiary hospital in northern Spain. Antimicrob Agents Chemother. 2015;59:1334–6.
44. Matsumura Y, Peirano G, Devinney R, et al. Genomic epidemiology of global VIM-producing Enterobacteriaceae. J Antimicrob Chemother. 2017;72:2249–58.
45. Pournaras S, Ikonomidis A, Tzouvelekis LS, et al. VIM-12, a novel plasmid-mediated metallo-beta-lactamase from *Klebsiella pneumoniae* that resembles a VIM-1/VIM-2 hybrid. Antimicrob Agents Chemother. 2005;49:5153–6.
46. Miriagou V, Tzouvelekis LS, Flevari K, et al. Providencia stuartii with VIM-1 metallo-beta-lactamase. J Antimicrob Chemother. 2007;60:183–4.
47. Lee HW, Kang HY, Shin KS, et al. Multidrug-resistant Providencia isolates carrying blaPER-1, blaVIM-2, and armA. J Microbiol. 2007;45:272–4.
48. Shin KS, Han K, Lee J, et al. Imipenem-resistant Achromobacter xylosoxidans carrying blaVIM-2-containing class 1 integron. Diagn Microbiol Infect Dis. 2005;53:215–20.
49. Lee MF, Peng CF, Hsu HJ, et al. Molecular characterisation of the metallo-beta-lactamase genes in imipenem-resistant Gram-negative bacteria from a university hospital in southern Taiwan. Int J Antimicrob Agents. 2008;32:475–80.
50. Figueiredo S, Poirel L, Papa A, et al. First identification of VIM-4 metallo-beta-lactamase in *Acinetobacter* spp. Clin Microbiol Infect. 2008;14:289–90.
51. Libisch B, Giske CG, Kovács B, et al. Identification of the first VIM metallo-beta-lactamase-producing multiresistant *Aeromonas hydrophila* strain. J Clin Microbiol. 2008;46:1878–80.

52. Tsakris A, Ikonomidis A, Spanakis N, et al. Characterization of In3Mor, a new integron carrying VIM-1 metallo-beta-lactamase and sat1 gene, from *Morganella morganii*. J Antimicrob Chemother. 2007;59:739–41.
53. Papagiannitsis CC, Verra A, Galani V, et al. Unravelling the features of success of VIM-producing ST111 and ST235 *Pseudomonas aeruginosa* in a Greek Hospital. Microorganisms. 2020. https://doi.org/10.3390/microorganisms8121884.
54. Papagiannitsis CC, Medvecky M, Chudejova K, et al. Molecular characterization of carbapenemase-producing *Pseudomonas aeruginosa* of czech origin and evidence for clonal spread of extensively resistant sequence type 357 expressing IMP-7 metallo-β-Lactamase. Antimicrob Agents Chemother. 2017. https://doi.org/10.1128/AAC.01811-17.
55. Zhao W, Hu Z. Epidemiology and genetics of VIM-type metallo-β-lactamases in Gram-negative bacilli. Future Microbiol. 2011;6:317–33.
56. Tseng SP, Hsueh PR, Tsai JC, et al. Tn6001, a transposon-like element containing the blaVIM-3-harboring integron In450. Antimicrob Agents Chemother. 2007;51:4187–90.
57. Di Pilato V, Pollini S, Rossolini GM. Tn6249, a new Tn6162 transposon derivative carrying a double-integron platform and involved with acquisition of the blaVIM-1 metallo-β-lactamase gene in *Pseudomonas aeruginosa*. Antimicrob Agents Chemother. 2015;59:1583–7.
58. Valot B, Rohmer L, Jacobs MA, et al. Comparative genomic analysis of two multidrug-resistant clinical isolates of ST395 epidemic strain of pseudomonas aeruginosa obtained 12 years apart. Genome Announc. 2014. https://doi.org/10.1128/genomeA.00515-14.
59. Yu T, Yang H, Li J, et al. Novel chromosome-borne accessory genetic elements carrying multiple antibiotic resistance genes in *Pseudomonas aeruginosa*. Front Cell Infect Microbiol. 2021;11:638087.
60. Pansegrau W, Lanka E, Barth PT, et al. Complete nucleotide sequence of Birmingham IncP alpha plasmids. Compilation and comparative analysis. J Mol Biol. 1994;239:623–63.


## Publisher's Note